Authors' accepted manuscript
Article published in *Metallurgical and Materials Transactions B* (2022)
The final published version is available at https://doi.org/10.1007/s11663-022-02437-1

Kinetic Simulation of Hot Metal Pretreatment: Desulphurization Using Powder Injection

Elmira Moosavi-Khoonsari[1], Marie-Aline Van Ende[2] and In-Ho Jung[2]

[1]Department of Mechanical Engineering, École de Technologie Supérieure (ÉTS), Montreal, Quebec H3C 1K3

[2]Department of Materials Science and Engineering and Research Institute of Advanced Materials, Seoul National University, Seoul, Republic of Korea, 08826

Corresponding author: Elmira Moosavi-Khoonsari

Tel: +1(514)396-8800 (ext. 8702)

E-mail: elmira.moosavi@etsmtl.ca

Submitted to

Metallurgical and Materials Transactions B

December 14th, 2021

Abstract

A kinetic model for hot metal pre-treatment process was developed. The co-injection of soluble magnesium and insoluble lime, and both of the transitory and permanent contact reaction zones were considered in the present model. That is, the model covers all the general features of hot metal desulfurization in the submerged powder injection, practiced at steel plants. The model was based on the effective equilibrium reaction zone approach in combination with FactSage thermodynamic databases. The process was divided into a finite number of reaction zones, and effective reaction volumes of each reaction zone were determined as a function of process parameters based on physical descriptions of reactions' mechanisms. The present model can be applied to a wide range of HM and top slag chemistries, and can calculate compositional evolution of both hot metal and slag during the process. The accuracy of model was compared to the sampled plant data. The current model was also utilized to study the potential for further optimization of the existing hot metal pretreatment process at a steel pant.

Keywords: Hot Metal Pre-treatment, Submerged Powder Injection, Thermodynamics, Kinetics, Effective Equilibrium Reaction Zone, Lime, Magnesium

1. Introduction

Sulfur in molten iron is typically originated from coke used in the ironmaking process. Usually, sulfur is not a beneficial element for steel quality, and its content should be tightly controlled during the iron and steelmaking processes. Although most of sulfur (about 90%) is removed in the blast furnace (BF), the sulfur content of hot metal (HM) from the BF varies widely between about 100 and 700 ppmw, which should be further reduced in some cases below 20 ppmw, *e.g.* in case of hydrogen induced cracking resistant steel.[1-4] The main purpose of hot metal pretreatment (HMP) is refining of HM from impurities including sulfur via strong chemical reactions between HM, refining flux, and carryover slag. Although sulfur could be further removed in the secondary refining process, desulfurization in HMP is more efficient and cost-effective.

Due to a growing demand to produce new steels with improved physical and mechanical properties and the increasing price of high-quality raw materials, more efficient desulfurization techniques need to be developed. In addition, reducing energy consumption and green house gas emissions remain as future challenges for steel producers. Hence, new processes are currently under development, producing HMs with different qualities such as sulfur and silicon contents, affecting the desulfurization efficiency.

Models coupling thermodynamics of a system and kinetic descriptions of a process are not only cost- and time-effective and aid in reducing trials and errors in plant operation, but also give reasonable predictions for process scenarios practiced out of their usual operation windows. The schematic diagram of HM desulfurization process using powder injection technology is presented in Figure 1. In general, the desulphurization reaction happens

mainly in the transitory reaction zone. However, as the removal and stabilization of sulfides after the desulfurization reaction occurs in the permanent contact reaction zone, consideration of this zone, involving top slag, is also very important to simulate the HMP process.

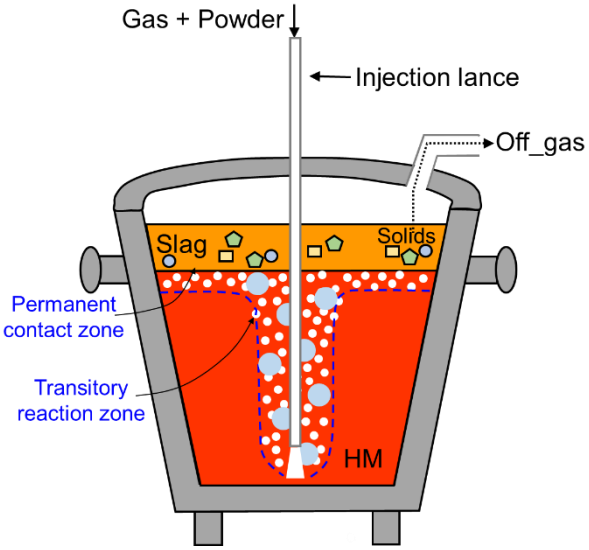

Fig. 1–Schematic diagram of hot metal pretreatment with powder injection.

Many researchers have investigated the desulfurization process by coupling experimental and modeling approach[5-10] considering only transitory reaction zone, or both zones. Several key literatures are briefly introduced here. Irons and Guthrie[5,6] studied the kinetics of desulfurization reaction between Mg vapor and HM in the transitory reaction zone using a mass transfer model based on single bubbles at the constant temperature of 1250 °C. They injected Mg vapor through a lance to 60 kg HM at 1250 °C and measured the changes in S and Mg contents during the injection process. Then, the desulfurization phenomenon at the interface of HM, MgS inclusion and bubble was analyzed. In their model, the thermodynamics of Mg dissolution[5,6] and desulfurization reaction[11,12] were considered.

Top slag was not considered in their study. Ohguchi and Robertson[7] studied the kinetics of desulfurization using a CaO-based flux, which is liquid at the steelmaking temperature and insoluble in the molten metal. The contribution of both transitory and permanent contact reaction zones to desulfurization was taken into account. The desulfurization by top slag was considered via the sulfide capacity of top slag.[7] They also developed a mixing model which was applied to the metal-slag reactions with a fixed slag volume.[13] However, in their model, the CaO-based flux ($CaO-Al_2O_3-CaF_2$) was considered for powder injection and the slag was assumed to be in the fully liquid state. Kitamura et al.[8] adapted the basic principles of a coupled reaction model by Ohguchi et al.[7] with some modifications to consider the influence of flux injection rate. They considered both the transitory and permanent contact reaction zones. A mathematical model considered phase equilibria and kinetics of the reactions in a ladle, and was applied to evaluate the removal of sulfur, phosphorous, silicon and manganese of HM. They presented the results only for the insoluble flux particles $CaO-FeO_x-CaF_2$. That is, desulfurization reaction using the soluble Mg flux was not modeled. They implied that the model could calculate compositional changes of liquid metal, flux and top slag during HMP. To calculate the chemical equilibrium, the activity coefficient of each component in the top slag, flux and metal was taken from different sources: (a) regular solution model of Ban-Ya et al.[14] for slag and flux particles, (b) sulfide capacity model of Sosinsky and Sommerville[15] for sulfur in the slag, and (c) the multicomponent dilute solution model[16] for liquid metal. One of possible limitations of the model is the assumption of homogeneous well mixed liquid metal (entire HM) during the process, which implies that liquid HM in the ladle could be completely homogenized within the simulation time step. Yang et al.[9] performed desulfurization

experiments using Mg vapor produced in-situ from carbothermic or aluminothermic reduction of MgO pellets, and modeled desulfurization process considering only the transitory reaction zone. However, this is far from an industrial HMP process. Recently, Visser[10] developed a model for desulfurization of HM considering the transitory reaction zone with Mg and lime injection. The gas flow rate and flux injection rate could be varied in the model to adapt to a specific plant need. They compared the simulation results with sampled plant data. In their simulation, they optimized the lime amount in contact with HM, and the Mg dissolution ratio in HM to reproduce the sampled plant data. Analysis of the plant samples revealed that the evolution of desulfurization products by using Mg and CaO powders is a two-stage process: (i) Mg + S → MgS inside the HM bath, and (ii) MgS + CaO → MgO + CaS in the upper layer of HM bath. That is, a simple approach considering only transitory reaction zone is insufficient to explain the desulfurization process of HMP. It can be concluded that both transitory zone with injected powders and permanent contact reaction zone with top slag are necessary for a complete desulfurization model description. However, the role of top slag was not considered in the model by Visser. [10] Moreover, the silicon oxidation, which was clear from the plant data, was not considered in their model.

In the current study, a kinetic process model was developed which can explain all the general features of the HM desulfurization route, practiced commercially worldwide at steel plant (*i.e.* the co-injection of soluble Mg and insoluble lime and both transitory and permanent contact reaction zones were considered in the present model). After reviewing the previous models in the literature,[5-10] a more complete description of reactions and fluid flow in transitory and permanent reaction zones were adapted in the present process model based on the effective equilibrium reaction zone (EERZ) concept.[17-21] A summary of

general features of the existing models in the literature is given in Table I in comparison to the current model and actual industrial operation. In addition, to apply the present model to a wide range of HM and top slag chemistries, thermodynamic calculations for local equilibria were performed using the FactSage thermodynamic databases[22] for liquid metal, solid and liquid slag containing sulfides, and gas phases. Partial solidification of slag phase could be also well calculated using the database. At the end, the current model was applied to study the potential for further optimization of the existing process at Tata Steel Europe.

2. Effective Equilibrium Reaction Zone Approach

In the EERZ model, [17] a complex process is divided into a finite number of reaction zones. For example, in the simple case of a slag – metal reaction, as shown in Figure 2, the

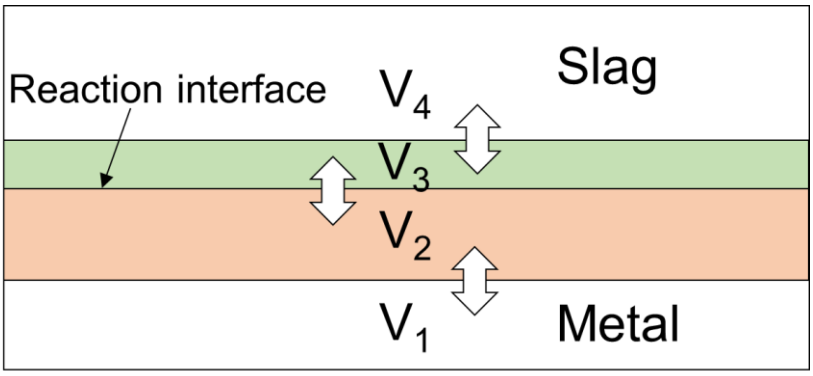

Fig. 2–Effective equilibrium reaction zone (EERZ) concept for slag – metal reaction.

metal phase would be divided into a bulk volume V1 and a smaller volume near the slag – metal interface V2. The slag phase would be divided in a similar way V3 and V4. In the EERZ model, it is assumed that all chemical reactions reach equilibrium in the chosen effective reaction volumes near the reaction interfaces. The equilibrium would be first calculated between V2 and V3, followed by equilibrium homogenization reactions in the metal phase (between V1 and V2) and in the slag phase (between V3 and V4). Kinetics are considered by varying the reaction zone volumes depending on physical descriptions of different reaction mechanisms, process conditions and the rate of homogenization in the slag and metal. Simplified mathematical functions and empirical relations derived from simulations, experimental studies and plant data can be used to describe the effective reaction zone volumes. This method allows for using the full potential of thermodynamic databases and an easy connection of thermodynamic databases to the kinetic simulation. The EERZ concept has been already used to simulate several metallurgical processes such as Rurhstahl-Heraeus vacuum degassing,[17] Basic Oxygen Furnace,[18] mold flux composition changes during the continuous casting,[19] the ladle furnace[20] and the mold slag – refractory – steel thermochemical interactions in and around the submerged entry nozzle in continuous casting.[21]

3. Kinetic Model for Hot Metal Pretreatment

3.1. Desulfurization Reactions with Injection of Metallic Magnesium and Lime

Among various desulfurization techniques, the co-injection of Mg and CaO is operated world-wide and considered a standard practice in North America and Europe. The Mg granules, lime powder and a carrier gas mostly N_2 are injected via a submerged lance into the HM ladle where together they form a bubble plume. The HM desulfurization occurs in the so-called transitory and permanent contact reaction zones as shown in Figure 1. In the transitory contact reaction zone within the bubble plume, the dissolved sulfur reacts with the injected desulfurization agents to form sulfide particles, ascending together with unreacted flux particles with the aid of bubble plume towards the top slag. Across the permanent contact reaction zone at the metal – top slag interface, further desulfurization reactions can occur, and desulfurization products are absorbed by the slag. At the end of the process, the slag is skimmed off, and the HM is transferred to the oxygen steelmaking converter.

The main desulfurization reactions happening in the transitory and permanent contact reaction zones are given in Eqs. [1] and [2], respectively:

$$[Mg] + [S] = MgS(s) \quad [1]$$

$$MgS(s) + (CaO) = (MgO) + (CaS) \quad [2]$$

where [ ] and ( ) stand for the component in hot metal and slag, respectively. In addition, CaO-rich slag can react with HM for desulfurization at the permanent contact reaction zone.

Magnesium reacts with sulfur to form MgS as shown in reaction [1]. However, desulfurization using Mg is challenging since MgS reacts with oxygen from air or other sources based on reaction [3], and as a result, resulfurization can occur. Therefore, lime is added as the sulfur stabilizer in the slag phase. Then, MgS absorbed to the top slag reacts with CaO to form CaS and MgO according to reaction [2]. Calcium sulfide is more stable than MgS and avoids the sulfur draw back to metal because of oxidation.

$$MgS(s) + 1/2O_2(g) = MgO(s) + [S] \quad [3]$$

According to the stoichiometric reaction [2], one mole of CaO is required per one mole of MgS, equal to CaO/Mg mass ratio of 2.3/1.0. However, it was reported that due to incomplete mixing, a higher ratio of CaO/Mg is required to prevent resulfurization.[10]

In addition to the above-mentioned reactions, the direct CaO desulfurization reaction can also happen in the plume, depending on the CaO particle size, according to reaction [4]:

$$CaO(s) + [S] = CaS(s) + [O] \quad [4]$$

where [ ] denotes the species dissolved in HM. However, it was reported that merely a fraction of lime particles contacts the metal at the metal – bubble interface and reacts with sulfur to form a CaS layer surrounding the lime particle. Once CaS layer forms, further chemical reactions to transform CaO(s) to CaS(s) is difficult because of slow solid-state diffusion process of sulfur through the CaS layer.[10]

On top of the main desulfurization reactions given in Eqs. [1], [2] and [4], accessory deoxidation reactions with C, Si and Mg could also occur:

$$[C] + [O] = CO(g) \quad [5]$$

$$[Si] + 2[O] = SiO_2(s) \quad [6]$$

$$Mg(g) + [O] = MgO(s) \quad [7]$$

These oxidation reactions result in partial HM decarburization and desiliconization, and part of Mg is removed by oxidation before it reacts with sulfur. Moreover, reaction [6] leads to the formation of $(CaO)_x \cdot (SiO_2)_y$ complex layer around the CaO particles, decreasing the sulfur diffusivity and reactivity.[10] In general, although such oxidation reactions rarely happen due to lack of dissolved oxygen in carbon-saturated HM, the reoxidation of HM by air due to open eye formation can still induce such reactions near the permanent contact zone.

3.2. Kinetics of Hot Metal Pretreatment Model

3.2.1. Overview of model

The HM desulfurization process was modeled using thermodynamics of the reactions, mass transfer coefficients in metal, slag and flux, and mass balance of components. Although heat balance could be considered in the EERZ approach, the present study assumed isothermal condition because no temperature profile of HM was measured in the plant. The schematic of the reaction zones in the current model is presented in Figure 3. As mentioned before, the process is divided into the so-called transitory and permanent contact reaction

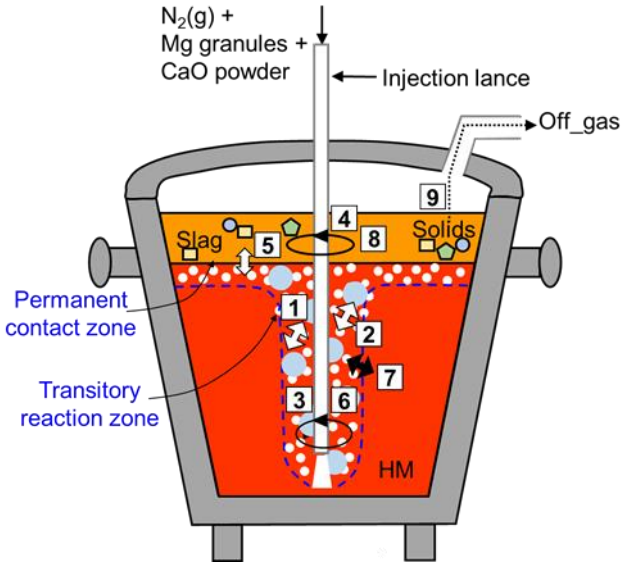

Fig. 3–Schematic diagram of the reaction zones in the present model of hot metal pretreatment (powder injection process).

zones. In the co-injection of Mg and lime, the transitory reaction zone is divided into 3 effective reaction zones (R1 to R3) as follows:

229 R1: plume and dissolved Mg reaction

230 R2: plume and lime particle reaction

231 R3: homogenization in plume

232 Four effective reaction zones (R4 to R8) were also defined in the permanent contact
233 reaction zone:

234 R4: first homogenization of top slag

235 R5: plume and top slag reaction including oxidation by air

236 R6: homogenization in plume

237 R7: homogenization of top slag

238 R8: exchange reaction between the plume and the remaining HM

239 R9: gas out

240 Thermodynamic equilibrium at each reaction zone was computed using the FactSage
241 thermochemical software version 7.3.[22] For the thermodynamic calculations,
242 thermochemical descriptions of the HM and slag phases (solid and liquid) were considered
243 from the FactSage FTmisc-FeLQ and FToxid databases, respectively. Thermodynamic
244 properties of gas phase and pure species were adopted from FactPS database.

245 The overall calculation procedure of the model has been shown in Figure 4. The program
246 calculates all the chemical reactions one by one in the order of reaction numbers at each

time step. The EERZ volume for each reaction is determined from simplified mathematical functions and empirical relations derived from the fluid dynamics simulation and plant data available in the literature. A number of user defined parameters, the plume height H_p, plume volume correction factor C, mixing time correction factor α, and excess oxygen for silicon oxidation are also included in the model, which might be adjusted to reproduce plant data, as listed in Table II.

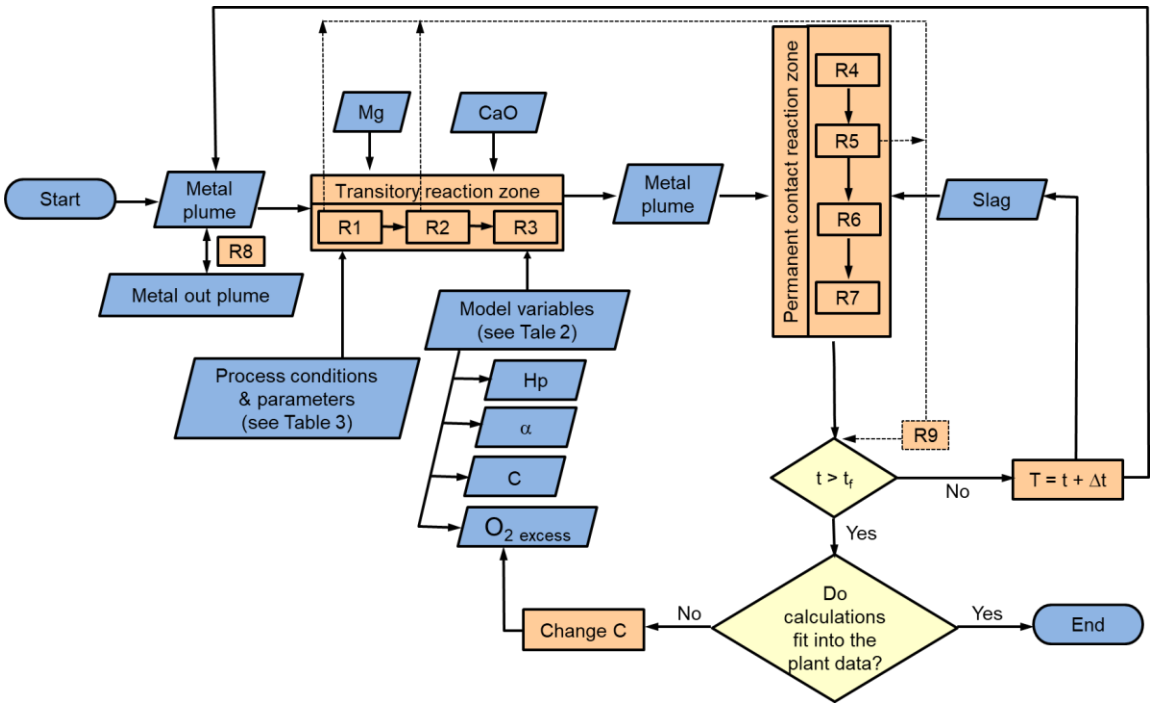

Fig. 4–The overall calculation procedure of the presented model.

3.2.2 Transitory Reaction Zone

The injected carrier gas, flux particles and liquid metal together form the bubble plume. Desulfurization occurs in the bubble plume via the flux and HM interaction. Therefore, the

plume dimensions must be known to calculate the effective HM volume reacting with Mg and lime. The plume radius for a bottom blown ladle was determined by Lachmund et al. [23] and Ebneth and Pluschkell.[21] Lachmund et al.[23] measured the plume radius only as a function of gas injection rate, but did not provide the change of the radius with height. Ebneth and Pluschkell[21] provided a more comprehensive description of a plume radius as a function of both gas flow rate Q and vertical coordinate x:

$$\delta = 0.38CQ^{0.15}x^{0.62} \quad [8]$$

where δ is the plume radius, C is a constant to adjust missing experimental data in the metal – gas system. For water, C was assumed to be equal to 1.0. In this study, this description of plume radius was adopted.

The schematic geometry of the bubble plume envisaged in this work is shown in Figure 5.

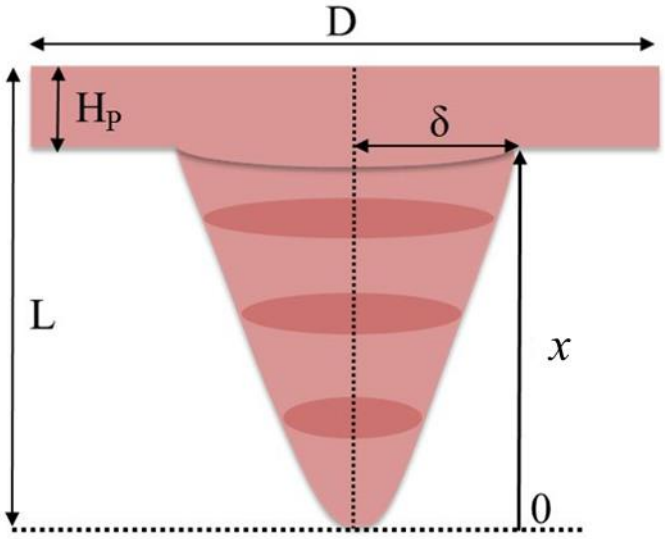

Fig. 5–Schematic presentation of the bubble plume.

The plume volume was calculated from the integration of the cross-sectional surface area of the plume by height and upper layer zone:

$$V_P = \frac{(0.38)^2 \pi C^2}{2.24} Q^{0.3} (L - H_P)^{2.24} + \frac{\pi}{4} D^2 H_P \quad [9]$$

where V_P and H_P are the plume volume and upper height, respectively, D is the metal bath diameter, and L the lance immersion depth.

3.2.2.1. Reaction between Hot Metal and Metallic Magnesium (R1)

For sulfur removal using Mg injection, two desulfurization mechanisms were proposed in the literature:[5, 6, 9, 25, 26] desulfurization at MgS inclusion sites and desulfurization at the bubble – metal interface. Desulfurization kinetics using Mg vapor injection was studied by Irons and Guthrie[5] in a 60 kg ladle. They reported that only 1-10% of desulfurization happens at the Mg bubble – metal interface where sulfur reacts with Mg vapor to form MgS, which is sheared off from the bubble surface by hydrodynamic shear force. Due to high vapor pressure of Mg in the bubble, Mg can be continuously dissolved into HM, and the dissolved Mg [Mg] can react with soluble sulfur [S], heterogeneously, at MgS inclusion sites which can be stripped off from the bubbles.[5, 6, 9, 11, 27] Yang et al.[9] and Mukawa et al.[25] investigated desulfurization kinetics using Mg vapor in 350 g and 30 kg metal baths, respectively. They reported that desulfurization at the Mg bubble interface is the main

sulfur removal mechanism. Lindström et al.,[26] who studied desulfurization kinetics in a 250 g size sample, reported that Mg slowly dissolves in the metal bath and then reacts with sulfur at MgO and/or CaO sites to form MgS. They only observed the MgS-MgO multiphase particles. Rarely any single MgS particle was observed in the bath, suggesting that MgS did not form via homogeneous nucleation. The MgO seeds resulted from the oxide layer around the Mg granules or the Mg oxidation by dissolved oxygen in the bath. Visser[10] recently studied desulfurization kinetics of HM during the co-injection of lime and Mg. Time series of two industrial heats were sampled followed by chemical and microstructural analysis. He confirmed the HM heterogeneous desulfurization mechanism at inclusion sites proposed by Irons and Guthrie.[5] However, the accumulation and floatation of MgS particles were different. Irons and Guthrie[5] observed only one MgS particle in a 1 mm^2 surface area but, the concentration of MgS particles observed by Visser[10] was noticeable, varying based on the sulfur and Mg concentrations in the melt. Individual MgS particles were observed by Visser[10] opposite to finding by Lindström[26] reporting MgS as part of the MgS-MgO assemblage. In the pilot scale induction stirred furnace (60 kg metal bath desulfurized for 60 min), mixing is better, and the floatation rate of MgS particles is higher than that in industrial operation (~300 ton metal bath desulfurized for 10 min). Visser[10] also mentioned that the overall efficiency of injected Mg in an industrial ladle is higher than that in a small-scale ladle. In an industrial ladle, the residence time of Mg in the metal bath is longer and the ferrostatic pressure at the injection point results in a higher vapor pressure of Mg increasing the driving force for the Mg dissolution.

Both dissolution of Mg in HM and the mass transfer of sulfur and magnesium to the nucleation sites have been reported as rate controlling steps for desulfurization of HM by Irons and Guthrie,[5] Lindström et al.[26] and Visser[10] for pilot scale, lab scale and real plant data, respectively. However, it can be assumed that mass transfer in a ladle heavily stirred using a carrier gas is fast enough, and can be ruled out as a rate controlling step. Irons and Guthrie[5] also reported that MgS inclusions are very tiny therefore, mass transfers of sulfur and magnesium could not be the main rate controlling steps. Hence, the dissolution rate of magnesium in HM can be the rate controlling step in real powder injection process, which was set equal to the magnesium fraction dissolved in the HM. This is called "magnesium efficiency (η_{Mg})".[10] The solubility product of MgS (P_{MgS} = *[ppmw Mg] [ppmw S]*) in HM is also very important in desulfurization using magnesium.

Based on the literature data, we assumed that the dissolution of Mg in HM happened first, and subsequently desulphurization reaction between [S] and [Mg] in HM was allowed. Different solubility products in carbon-saturated liquid iron were reported in the literature.[5, 28-30] In this work, the MgS solubility product, P_{MgS}, for the given HM composition (see Table III) was calculated in the temperature range 1250 - 1450 ^{o}C at 1 atm total pressure using FactSage 7.3 (FTmisc FeLq and FactPS databases). The predicted solubility products using FactSage are plotted in Figure 6 along with the results given by Turkdogan.[28] As it is seen, there is good agreement between the FactSage calculations and data from Turkdogan.[28] It can be implied that the difference in the calculated Mg solubility by FactSage and Turkdogan is very small. For example, at 1450 ^{o}C, the equilibrium Mg content in HM for heat 1 (203 ppm S) and heat 2 (229 ppm S) was

calculated by FactSage to be about 10 and 9.4 ppm, respectively, in comparison to 9.7 and 8.6 ppm from Turkdogan, respectively.

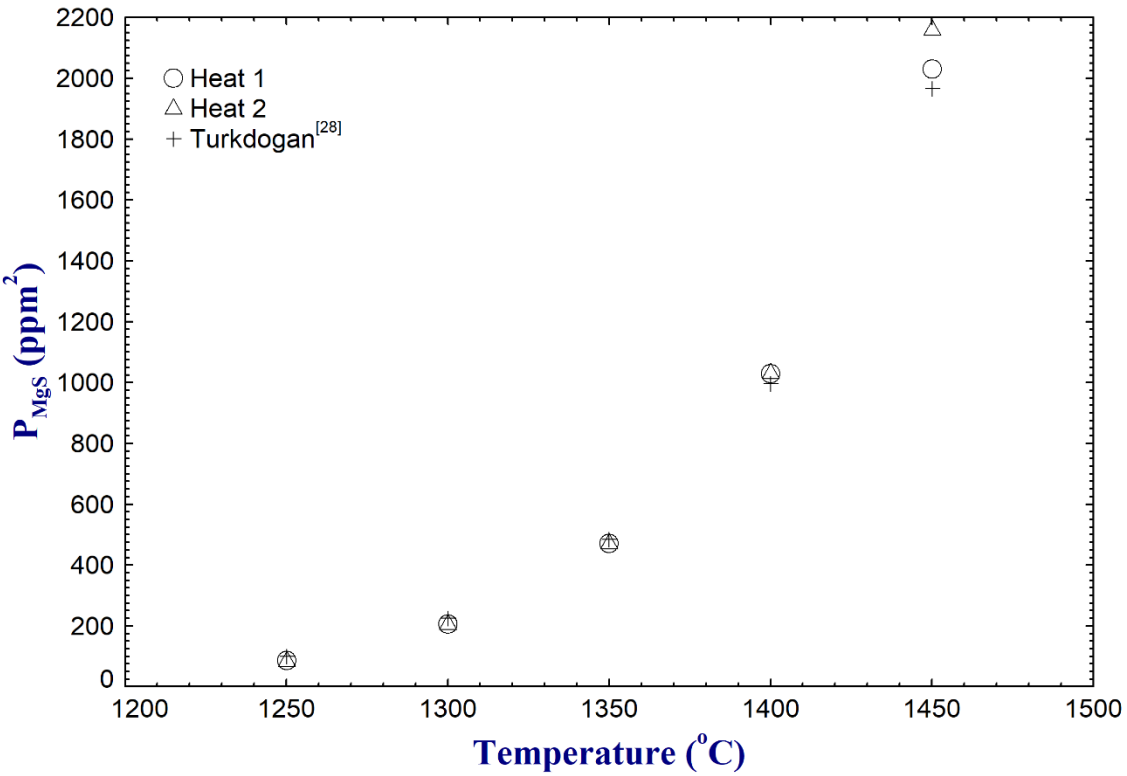

Fig. 6–Solubility product of MgS, P_{MgS} = *[ppmw Mg] [ppmw S]*, in hot metal calculated using FactSage 7.3. Compositions of heat #1 and heat #2 are given in Table III.

The solubility product P_{MgS} can be also described by the average Eq. [10]:

$$Log P_{MgS} = -64.52288 + 21.469 \text{ Log T}(°C) \quad [10]$$

A wide range of magnesium efficiency (10% - 80%) was reported for the hot metal desulfurization based on laboratory scale experiments and industrial trials.[5, 10, 26, 31-37] The

low efficiency of magnesium is pertinent to its reaction with air from the spout area, incomplete dissolution of magnesium in HM, its evaporation to off-gas, and its reaction with SiO_2 and Al_2O_3 in top slag according to the reactions below:

$$(SiO_2) + 2Mg(g) = 2(MgO) + [Si] \quad [11]$$

$$(Al_2O_3) + 3Mg(g) = 3(MgO) + 2[Al] \quad [12]$$

In the present model, η_{Mg} is an adjustable model parameter which can be entered directly as an input of the model considering plant data. The overall magnesium efficiency η_{Mg} is calculated from the amount of magnesium dissolved in the HM and bound to MgS after injection relative to the total amount of magnesium injected:

$$\eta_{Mg} = \frac{\left([ppm\ Mg]_d + \frac{M_{Mg}}{M_S}\Delta[ppm\ S]_d\right)\cdot m_{HM}}{1000000\ m_{Mg-T}} \quad [13]$$

where $[ppm\ Mg]_d$ is the dissolved magnesium content in the HM after injection, $\Delta[ppm\ S]_d$ indicates the difference between the final and initial dissolved sulfur contents in HM, m_{HM} and $m_{Mg\text{-}T}$ are the total mass of HM and injected Mg, and M_{Mg} and M_S magnesium and sulfur molecular weights, respectively.

In the present study, one equilibrium calculation was performed between the metal plume (see Eq. [9]) and Mg considering η_{Mg} from Eq. [13]. That is, the amount of HM in the

plume and Mg amount were added as inputs for R1 calculation, and the outputs of reaction R1 are new HM in plume zone and MgS inclusion.

3.2.2.2. Hot Metal and Lime Particle Reaction (R2)

The effective reaction zone volumes of bulk metal V_m^t and lime particles V_p^t in the transitory reaction zone are determined as follows:

$$V_m^t = k_m^t\left(n_p A_p\right)\rho_m \Delta t \quad [14]$$

$$V_p^t = k_p^t\left(n_p A_p\right)\rho_p \Delta t \quad [15]$$

where k_m^t and k_p^t are the overall mass transfer coefficients in the bulk of metal and lime particle, n_p and A_p the number of lime particles injected and single particle surface area, ρ_m and ρ_p the metal and lime particle densities, respectively, and Δt is the calculation time step. The total surface area available for the metal – lime particle reaction is the product of $n_p A_p$. The number of particles is calculated from the particle injection rate W_p, particle residence time t_p, particle diameter d_p and particle density ρ_p:

$$n_p = \frac{6 W_p t_p}{\pi d_p^3 \rho_p} \quad [16]$$

The residence time of injected lime particles is calculated accordingly:

$$t_p = \frac{H}{U_m} \quad [17]$$

Due to the formation of bubble plume, it was assumed that the ascending velocity of lime particles and desulfurization products is equal to the metal mean rising velocity. The mean rising velocity of metal in the plume zone was determined from the numerical analysis of fluid flow and water model experiments as following: [8]

$$U_m = 19.9\left(Q/D^2\right)\left(gD^5/Q^2\right)^{0.24}\left(L/D\right)^{0.20}\left(H/L\right)^{0.52} \quad [18]$$

where g is acceleration due to gravity.

The mass transfer coefficient in the bulk metal k_m^t at the injected lime particle – metal interface is estimated as follows:[8]

$$k_m^t = 2\left({D_m u}/{\pi d_p}\right)^{1/2} \quad [19]$$

where D_m is the diffusion coefficient, here of sulfur, in the hot metal, and u is the slip velocity between the metal and lime particle which can be obtained from Allen's equation:[8]

$$u = \left(\frac{4(\rho_m - \rho_p)^2 g^2 d_p^3}{225 \rho_m \mu_m}\right)^{1/3} \quad [20]$$

where μ_m is the HM viscosity. The diffusion coefficients of sulfur in carbon-saturated liquid iron reported in the literature are different in orders of magnitude (from 10^{-6} to 10^{-9} m^2/s).[38-40] In this work, D_m can be adjusted.

Since the mass transfer coefficient in the top slag is assumed to be 1/10 of that in the metal [8] (as will be explained in section 3.2.3.1), the mass transfer coefficient in the solid particle k_p^t at the injected lime particle – metal interface is assumed to be 1/100 of that in the metal ($k_p^t = 1/100 k_m^t$).

According to Eq. [19], the mass transfer rate is inversely proportional to the square root of the lime particle diameter. Moreover, the lime particle size affects the interfacial reaction surface and subsequently the effective reaction volumes. In practice, a mixture of lime

particles within a certain size distribution is injected into the bath during the process however, in the model, only a fixed lime particle size is allowed. The average lime particle diameter of 110 μm calculated from the measured particle size distribution ($d_p^{average} = \sum_i d_{p,i} vol\%$) was entered as the model input in this study.

3.2.2.3. First Homogenization in the Plume (R3)

Full homogenization of chemistry and temperature of the metal plume was assumed at each calculation time step.

3.2.3. Permanent Contact Reaction Zone

3.2.3.1. Hot Metal and Top Slag Reaction (R5)

The permanent contact reaction zone accounts for the reaction between metal and top slag. The effective reaction zone volumes of metal V_m^p and top slag V_s^p for the permanent contact reaction zone are expressed as follows:

$$V_m^p = k_m^p A \rho_m \Delta t \quad [21]$$

$$V_s^p = k_s^p A \rho_s \Delta t \quad [22]$$

where k_m^p and k_s^p are the overall mass transfer coefficients in the bulk of metal and top slag, respectively. ρ_m and ρ_s are the densities of metal and top slag, respectively, A is the contact surface area between the metal and top slag and Δt is the calculation time step.

In the current model, ρ_m and μ_m were adjusted based on the HM temperature according to the following Eqs.:[41, 42]

$$\rho_m = \rho_m^o + [-0.883 \times 10^{-3}(T - T_m)] \quad [23]$$

$$\mu_m = 0.3699 \times 10^{-3} e^{\frac{41.4 \times 10^3}{RT}} \quad [24]$$

where ρ_m^o is the HM density at its melting point T_m, and R is the gas constant. The slag density was calculated from the partial molar volumes and molecular weights of slag components at 1400 °C.[43]

The overall mass transfer rate in the metal k_m^p at the metal – top slag interface is expressed as:[8]

$$k_m^p = 2.18 \times 10^{-3} \left(L^2 \varepsilon / D\right)^{1/2} \quad [25]$$

where L and D are the lance immersion depth and metal bath diameter, respectively, ε is the mixing energy, calculated from the equation suggested by Kai et al.:[44]

$$\varepsilon = 6.18 \times 10^{-3} \frac{QT}{W_m}\left\{2.303log\left(1 + \frac{\rho_m Lg}{1.01325\times10^5\times P^o}\right) + 0.06\left(1 - \frac{T_Q}{T}\right)\right\} \quad [26]$$

where W_m, P^o and T_Q are the metal weight, pressure on bath surface and gas temperature, respectively. Q and T are gas flow rate and metal bath temperature, respectively. To the knowledge of the authors, no mixing energy equation was reported for the top submerged lance injection, and different effects of the two configurations (top submerged lance and bottom blowing) on the fluid flow and mixing are not known. In the present study, therefore, we took Eq. [26], suggested by Kai et al.[44]

The mass transfer coefficient in the top slag is assumed to be 1/10 of that in the metal ($k_s^p = 1/10k_m^p$) since the diffusion coefficient of a component in the metal is 1 to 2 order larger than that in the slag.[8] Based on these mass transfer coefficients, the volume of HM and top slag reacted in R5 were determined. In addition, to consider the oxidation of Si in real plant data, we introduced a small amount of excess O_2 in R5 reaction. The amount of oxygen reacts with Si is optimized in the model to reproduce the Si profile in HM.

3.2.3.2. Hot Metal and Top Slag Homogenization (R3, R4, R6 – R8)

The plume was assumed to be always homogeneous in chemistry and temperature at each time step (R3 and R6) since it is heavily stirred by the carrier gas during the injection. Full homogenization of the top slag composition and temperature was also assumed at each calculation time step (R4 and R7) despite possible slag inhomogeneity.

The effect of mixing energy on the metal homogenization (R8) and the dead zone occurrence were considered in the present model. That is, if the mixing time t_{mix} was equal or shorter than the calculation time step ($t_{mix} \leq \Delta t_{calc\text{-}step}$), a full homogenization was assumed between the metal plume and the rest of the metal bath. Otherwise, if the mixing time was longer than the calculation time step ($t_{mix} > \Delta t_{calc\text{-}step}$), the bath homogenization rate depends on the metal mass exchanged between the plume and the remaining metal bath (*i.e.* the exchange mass becomes a model variable). The following input amounts of plume and remaining HM in ladle were considered in reaction R8 depending on the t_{mix} and $\Delta t_{calc\text{-}step}$:

$t_{mix} \leq \Delta t_{calc\text{-}step}$: $V_{\text{plume (R8)}} = V_{\text{plume total}}$, $V_{\text{Remaining HM (R8)}} = V_{\text{Remaining HM}}$ [27]

$t_{mix} > \Delta t_{calc\text{-}step}$: $V_{\text{plume (R8)}} = V_{\text{plume}} + V_{\text{Remaining HM-exchanged}}$, $V_{\text{Remaining HM (R8)}} = V_{\text{Remaining HM}} + V_{\text{plume-exchanged}}$; $V_{\text{Remaining HM\_exchange}} = V_{\text{plume-exchanged}}$ [28]

The resultant HM and plume from reaction R8 are transferred to the next time step.

Different equations for the mixing time were reported in the literature[45-52] mostly for a bottom blown ladle. In this work, the time required to achieve 95% mixing in the HM bath was used:[52]

$$t_{mix} = \left(25.4 \frac{(D/2)^{7/3}}{(\beta Q)^{1/3} H}\right) \quad [29]$$

where β is the fractional depth of lance submerged. Q and D are gas flow rate and metal bath diameter, respectively. Eq. [29] was developed by Mazumdar and Guthrie[52] from the water model experiments for a bottom blown ladle. However, Asai et al.[47] suggested using the correction factor α $(= \frac{\rho_m}{\rho_w})$ to count for the difference between the steel and water densities. Hence, the mixing time can be readjusted as follows:

$$t_{mix} = \alpha \left(25.4 \frac{(D/2)^{7/3}}{(\beta Q)^{1/3} L}\right) \quad [30]$$

In the present model, there is freedom to change α.

3.2.3.3. Gas out (R9)

501 This reaction is simply needed to check the mass balance of the entire process. All unused
502 Mg and injected N_2 gas exit the process via this reaction. No specific chemical reaction
503 was necessary.

504

505 *3.2.4. Main Assumptions in the Present Model*

506 The main assumptions and approximations made in the present study are as follows:

507 (a) No reaction occurred between the refractory linings and the fluids (metal and slag).

508 (b) No physical entrainment of metal in slag and vice versa was considered.

509 (c) All reaction products including MgS and CaS were absorbed by the top slag.

510 (d) Magnesium vapor instantly dissolved in the HM at the time it exited the lance tip and
511 was homogeneously distributed over the entire plume.

512 (e) The immobilization of the flux particle surface due to the presence of surface-active
513 elements was not considered.

514

515 **4. Application of the Model to Plant Operations**

516 **4.1. Plant Trial Data: Tata Steel Europe**

The developed kinetic model was tested against two plant data sets, which were collected during a special campaign at Tata Steel desulfurization station in IJmuiden, the Netherlands.[10] Usually, no samplings are carried out during the desulfurization process, but 6 to 8 samples of HM were taken during the campaign. At the beginning of HMP, when the lance was being lowered into the HM bath, the injection of N_2 carrier gas was started. Once the lance tip reached the depth of 0.5 m, the lime injection begun. When the conveying line was thoroughly cleaned, and all oxygen was flushed out, magnesium was co-injected with lime (< 6 min) followed by lime mono-injection (~ 1 – 2 min) to clear out the line from Mg and complete the MgS particle floatation. In total 117 – 144 and 728 – 732 kg of Mg and lime, respectively, were injected within 10 min of the process. The Mg and lime injection rates varied in the range 22 - 26 and 88 – 102 kg/min, respectively. The N_2 carrier gas was injected at a rate of 17 m^3/min at room temperature. HM samples were taken from the depth of 0.5 – 0.6 m below the surface. The first sample was collected just before the start of injection and the last sample was collected after the removal of the lance from the HM bath. More details about the campaign can be found elsewhere.[10]

4.2. Simulation Conditions

The initial conditions and process parameters of the two HM desulfurization processes used in the present simulations are listed in Table III. For the calculations, lime was added during the first 7 min, and Mg was added within 1 - 6 min of the process. The flux injection rate and timing are plotted in Figures 7(a) and 8(a) for heat #1 and heat #2, respectively. The total sulfur and Mg contents were measured by using X-ray fluorescence (XRF) and

scanning electron microscopy (SEM) coupled with energy dispersive spectroscopy (EDS). [10] However, soluble sulfur [S] and magnesium [Mg] contents were not directly measured. Therefore, [S] was derived in this study from the following equation using the total S and Mg contents:

$$[ppm\ S]_d^2 + \left(\frac{M_S}{M_{Mg}}[ppm\ Mg]_T - [ppm\ S]_T\right)[ppm\ S]_d - \frac{M_S}{M_{Mg}}P_{MgS} = 0 \quad [31]$$

where the subscripts T and d stand for total and dissolved elements, respectively. Magnesium and sulfur also bound together to form MgS particles in the HM. The solubility products for the HM conditions, given in Table III, were calculated to be about 577 and 915 ppm^2 at 1370 and 1399 °C, respectively. Similarly, the dissolved Mg content [Mg] was calculated. These [S] and [Mg] data are also plotted in Figures 7(a) and 8(a). Magnesium efficiency (η_{Mg}) was calculated to be 51 and 43% for heat #1 and heat #2, respectively, according to Eq. [13].

The overall pressure at the injection point was calculated from the summation of pressure on the bath surface (P^o) and ferrostatic pressure at the injection point:

$$P = P^o + \rho_m g L \quad [32]$$

558 The model variables that were fixed to reproduce the plant data are listed in Table II. The
559 lance depth in the plant was 3.2 m, and plume height (H_p) was estimated to be 0.2 m in the
560 simulation. The plume volume correction factor C was set to be 3.0. Using the correction
561 factor 1.0, the plume volume would be about 4 m^3 which seems to be very small in
562 comparison to 46 m^3 metal bath, which cannot reproduce the desulfurization profile as it
563 happens mainly inside the plume. With a correction factor of 3, the plume volume forms
564 about 26% of the total metal volume which not only sounds reasonable but also leads to
565 much better prediction of elemental profile of the HM for both heat series. The mixing time
566 correction factor (α) has its default value of 1.0 since the argument by Asai et al.[47] to
567 include the ratio of metal density/water density ($=\alpha$) into the mixing time equation [29]
568 was not supported by any experimental measurements.[53] In the present simulation, the
569 calculation time step (Δt) was set to be 1 min.

570 The main reaction zone volumes, mass transfer coefficients and mixing times of
571 importance for the present simulation were calculated and listed in Table IV. The time
572 required to achieve 95% mixing in a ladle with the specified dimensions and gas flow rate
573 0.28 Nm^3/s was calculated to be less than a minute (~0.9 min), the plume volume about 1/3
574 of total metal bath volume, and the particle residence time ~ 0.6 s. The ascending velocity
575 of desulfurization products including MgS and CaS can be reasonably set equal to the mean
576 rising velocity of metal in the bubble plume. All reaction products were assumed to float
577 up to the top slag.

578 It is found that the temperature of top slag is very critical for the evolution of phases in top
579 slag. The top slag chemistry can be continuously changed due to the chemical reaction with

HM and accumulation of the injected CaO and reaction products MgS and CaS in the plume zone. For example, the preliminary simulation results for heat #1 at 1370 ^{o}C isothermal condition (reported temperature by Visser[10]) showed that top slag became completely solid during the period of 4 to 7 minute after the beginning of injection process. In reality, the temperature of slag and HM would not be constant during the process. Unfortunately, Visser[10] did not report exact conditions of temperature measurement, and whether it was measured before or after the desulfurization process. Analysis of annual heat data at Tata Steel, IJmuiden revealed that HM temperature could decrease more than 30 ^{o}C during the desulfurization process. In the present simulation, considering the temperature drop in HM desulfurization process, the temperature of heat #1 was adjusted from 1370 ^{o}C to about 1400 ^{o}C during the first 6 min of the simulation to ensure the occurrence of the liquid slag. In the case of heat #2, simulation was performed at 1399 ^{o}C. It should be noted that such change in temperature of heat #1 does not significantly influence the variation of sulfur in HM except the phase evolution of top slag.

4.3. Simulation Results

The HM and slag concentration profiles calculated for heat #1 and heat #2 with the current model are shown in Figures 7 and 8, respectively, in comparison to the plant data. The plant data show that S content decreased when Mg injection began. The Mg and lime injection periods and amounts were also shown in the figures which can be read from the right y-axis. The initial conditions, process parameters and model variables are listed in Tables III and II. During the addition of Mg, the S content deceased from 200 ppmw to

about 20 ppmw within 5 minutes. As seen in Figures 7(a) and 8(a), the present model reasonably predicts the dissolved sulfur and magnesium contents of the HM during the process.

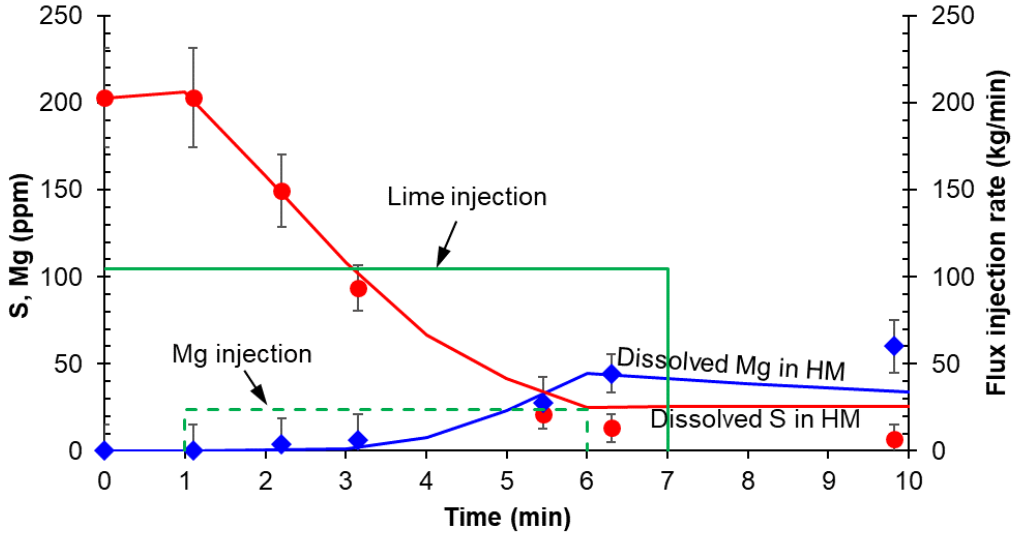

(a)

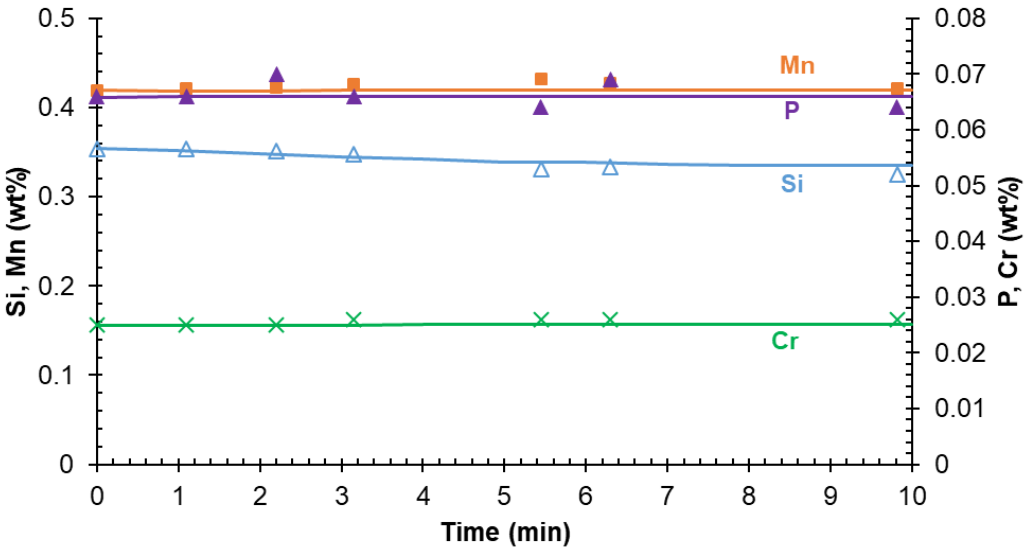

(b)

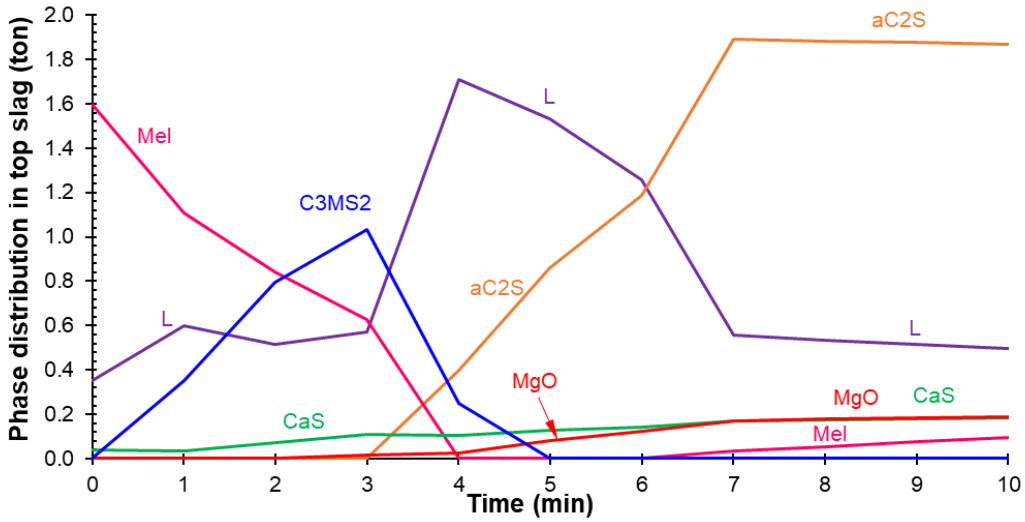

(c)

Fig. 7–Simulated heat #1 (a), (b) hot metal composition, and (c) phase distribution in top slag. The symbols are plant data.[10] The lines were calculated from the present model. L, Mel, aC2S and C3MS2 stand for liquid slag, melilite, α-C_2S and $Ca_3MgSi_2O_6$, respectively.

605

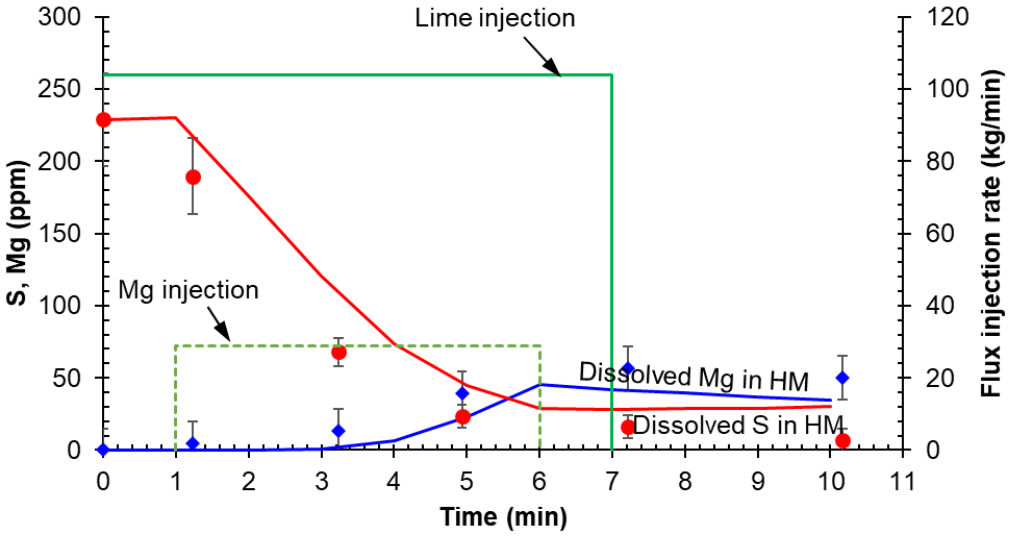

(a)

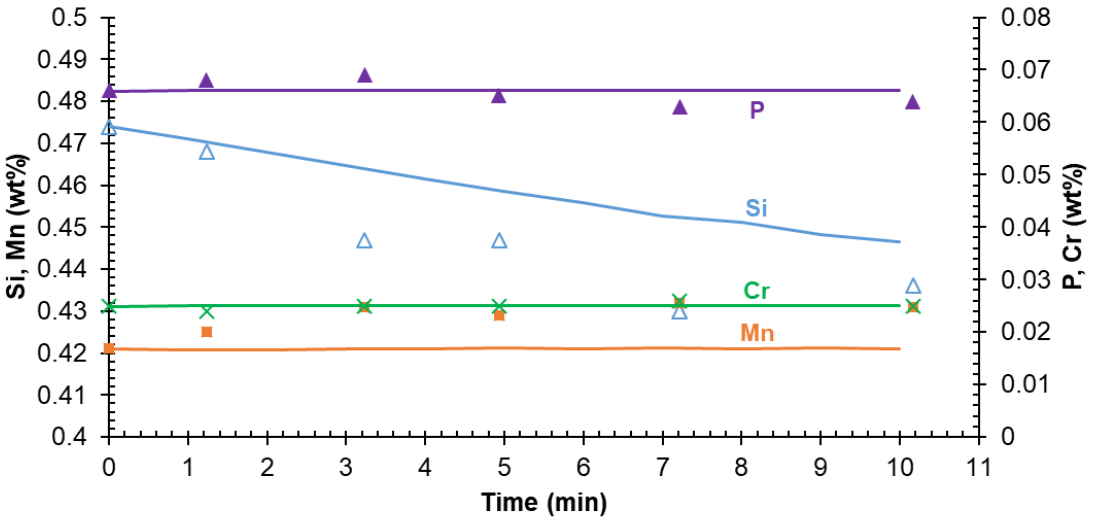

(b)

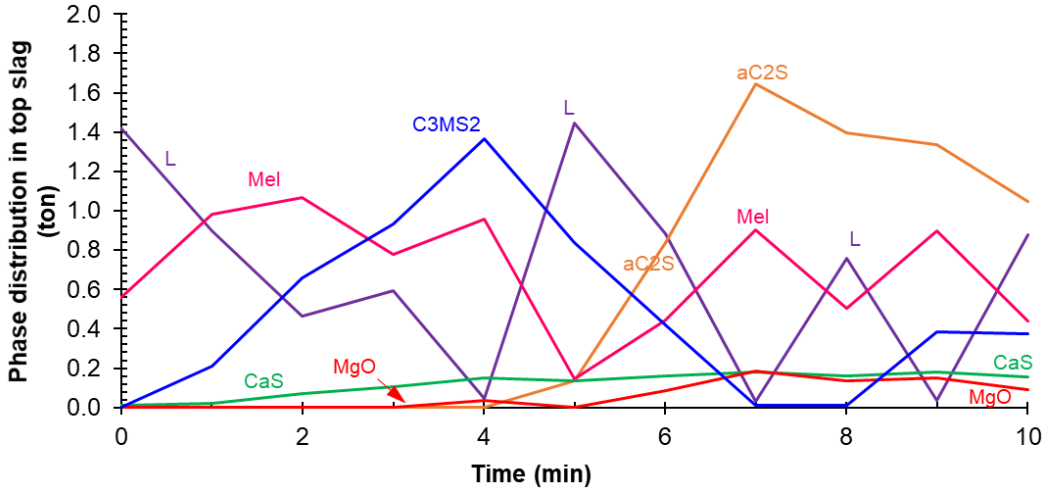

(c)

Fig. 8–Simulated heat #2 (a), (b) hot metal composition, and (c) phase distribution in top slag. The symbols are plant data.[10] The lines were calculated from the present model. L, Mel, aC2S and C3MS2 stand for liquid slag, melilite, α-C_2S and $Ca_3MgSi_2O_6$, respectively.

606

607 According to Figures 7(b) and 8(b), no dephosphorization and dechromization occur during

608 the process, in agreement with the plant data. In the preliminary calculation, we found that

609 the calculated Si content only slightly decreased by about 15 and 26 ppm during the

process, whereas a drop of 290 and 380 ppm in the Si content was measured at the plant, respectively. Even assuming that entire slag and HM are in equilibrium state, this decrease of Si cannot be explained. This means that there are other sources of oxygen for Si oxidation. When additional oxygen was included in the calculation, it was found that only Si could be oxidized, preferentially, among all other solute elements. Therefore, in the present simulation, a small amount of additional oxygen (0.01 kg/min) was considered in R5 reaction (permanent contact zone reaction) to account for the Si oxidation. The oxygen could be originated from air due to open eye formation during injection.

It is not possible to sample the slag during injection due to health and safety regulations and, at the end of the process because of high viscosity of the slag, which is indicative of high solid content of the slag (equivalent to low liquid fraction). Therefore, the real change in the slag chemistry/mineralogy is not known with certainty yet. However, the present model provides an estimation for the top slag evolution in a time series. As seen in Figures 7(c) and 8(c), the slag phase significantly varies during injection. Initially with lime addition, solid $Ca_3MgSi_2O_6$ stabilizes and sharply increases at the expense of the liquid phase and/or melilite. With the addition of metallic Mg, MgS desulfurization product reacts with CaO in the top slag and consequently MgO and CaS amounts increase according to reaction [2]. With further addition of lime and Mg, melilite decreases and α-C_2S starts forming. After lime injection (8 to 10 min), the simulated slag in heat #1 does not notably vary, as shown in Figure 7(c), however, the simulated slag in heat #2 still significantly changes, as depicted in Figure 8(c). The change in slag after the lime addition can be explained by considering the oxidization of Si in hot metal due to the formation of an open eye in the ladle during the process. The Si oxidation was incorporated in reaction R5, where

633 the top slag is equilibrated with hot metal plume. Therefore, a small amount of oxygen was
634 added in R5 during the process. Overall, a higher degree of Si oxidation might result in
635 more variations in slag. For example, for heat #2, liquid slag is transformed to solid α-C_2S
636 and melilite phase at 7 min due to the reaction with injected solid CaO. Then, liquid silicate
637 slag is regenerated by R5 reaction at 8 min due to the oxidation of Si in hot metal and
638 modified due to re-equilibration with existing solid slags in reaction R7. Subsequently, the
639 additional oxidation of Si and re-equilibration with the existing solid slags at 9 min can
640 produce more solid $Ca_3MgSi_2O_6$ and melilite phases. Afterward, liquid slag forms again at
641 10 min. At the end of the process, the model reveals that the BF slag transforms to a slag
642 rich in dicalcium silicate, which is consistent with the plant data.[54] The α-C_2S phase is the
643 solid solution of mainly Ca_2SiO_4 and Mg_2SiO_4 with small amounts of Fe_2SiO_4 and
644 Mn_2SiO_4.

645

646 The compositions of the end slag for heat #1 and heat #2 were missing in the original
647 campaign. In other campaigns, end slags were sampled and analyzed using XRF. The main
648 components of slag were (18 – 50) CaO, (16 – 47) SiO_2, (3 – 25) Al_2O_3, (8 – 17) MgO, (1
649 – 13) S, and (1 – 12) MnO in wt%. The variation in slag chemistry from heat to heat can
650 be related to not only different initial and process conditions of each heat sampled in the
651 plant but also inhomogeneous nature and sampling location of slag. The predicted
652 compositions of the end slag lie within the composition range of sampled slags. The
653 predicted slag composition for heat #1 and heat #2 are about 49 CaO, 22.5 SiO_2, 17 Al_2O_3,
654 8.5 MgO, 3 CaS in wt %.

655

656 **4.4. Roles of Magnesium and Lime Particles and Top Slag in Desulfurization Process**

657 The contribution of magnesium, lime and top slag to the sulfur removal process was
658 separately calculated from the present process model. Three simulations were performed
659 based on heat #1 operational conditions assuming (i) only Mg injection without lime and
660 top slag, (ii) only lime addition without Mg and top slag, and (iii) top slag without any flux
661 addition. In the simulations (i) and (ii) without top slag, the desulfurization products such
662 as MgS and CaS were allowed to stay at the top of HM and still react with HM. The
663 calculated results are presented in Figure 9. Considering the simulation results for all three
664 contributions, addition of only Mg can lead to 77 % of final desulfurization level. Addition
665 of only lime, 43% of final desulfurization level can be achieved. Having only top slag can
666 result in slight re-sulfurization of HM because of a decrease in sulfur distribution (L_S =
667 $(\%S)_{slag}$ / $[\%S]_{HM}$) with decreasing temperature from BF tapping (about 1550 ^oC) to
668 desulfurization station (about 1400 ^oC). It is also interesting to note the slight increase of
669 sulfur in the case of only Mg addition after 6 min. This is due to the re-equilibration of HM
670 by MgS products after the end of desulfurization in the transitory zone. That is, the
671 desulfurization in the transitory zone under ferrostatic pressure of HM is stronger than the
672 sulfur equilibration with MgS product at 1 atm, which indicates that the stabilization of
673 MgS by CaO explained in Eq. [2] is important to enhance the Mg desulfurization
674 efficiency.

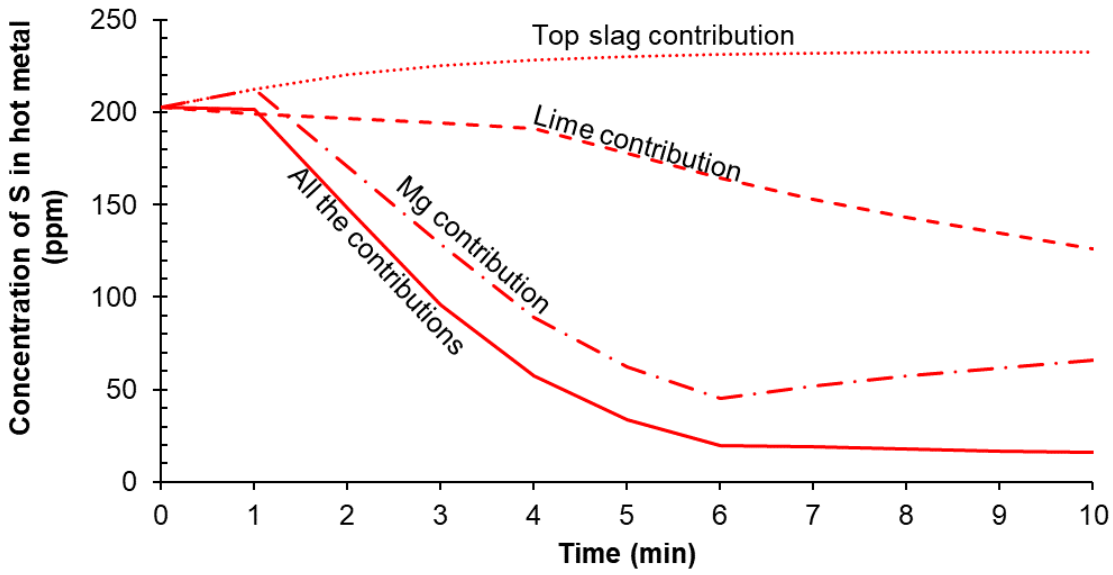

675

676 Fig. 9–Separate contribution of magnesium, lime and top slag to the sulfur removal
677 process, calculated from the present process model. Three simulations were performed
678 based on heat #1.

679

680 Although solid CaO powder can directly react with the solid MgS desulfurization product;
681 molten slag enriched with CaO has a more effective role in stabilization reaction of MgS.
682 Once solid MgS particles resulting from the chemical reaction of Mg and S at the transitory
683 zone float up to the surface of HM, liquid slag dissolves the solid particles and stabilizes
684 them. Without liquid slag, the solid MgS particles could bounce back into HM following
685 the fluid flow of liquid metal, and desulfurization would be less efficient. Therefore, the
686 presence of even small amount of liquid slag can be important. Formation of a complete
687 solidified slag for a short period of time during the desulfurization process would be
688 acceptable but not ideal. On the other hand, for skimming the final slag with minimum HM
689 entrainment loss after the end of process, having a slag with high solid fraction is more
690 preferable. To meet both these requirements, top slag composition should be carefully

691 determined. As can be seen from the two industrial cases, proper amounts of lime were
692 added to top slag to control the volume of slag liquid fraction.

693

694 **5. Applications of Model to the Optimization of Desulfurization Process**

695 It was shown that the developed model can reasonably predict the chemical composition
696 of HM during the desulfurization process (see Figures 7 and 8). Therefore, the present
697 kinetic model can be utilized to optimize the process conditions.

698 A common belief at HM desulfurization station is that often more than adequate amounts
699 of Mg and lime are injected at steel plant because penalty to be paid for high final sulfur
700 contents are higher than the costs of extra reagents (the costs associated to increased iron
701 losses due to higher volumes of top slag are often ignored).[54] Therefore, optimization of
702 amount of added flux is important to reduce the process cost. For this purpose, the present
703 model was used at Tata Steel IJmuiden along with many plant campaigns. Only one case
704 study of the simulation results is presented here.

705 Seven scenarios of HM desulfurization with different added amounts of flux were
706 simulated and the sulfur profile results are plotted in Figure 10. In the simulations, all the
707 process conditions with the exception of flux amounts were kept the same as that of heat
708 #1 in Table III. Scenario 1 represents the original practice of heat #1. Scenarios 2 and 3
709 present the cases with addition of half of and twice of the flux amount at the original
710 Mg/CaO ratio, respectively. Scenarios 4 and 5 represent the cases of half of and twice of
711 the amount of Mg with a fixed original amount of lime, respectively.

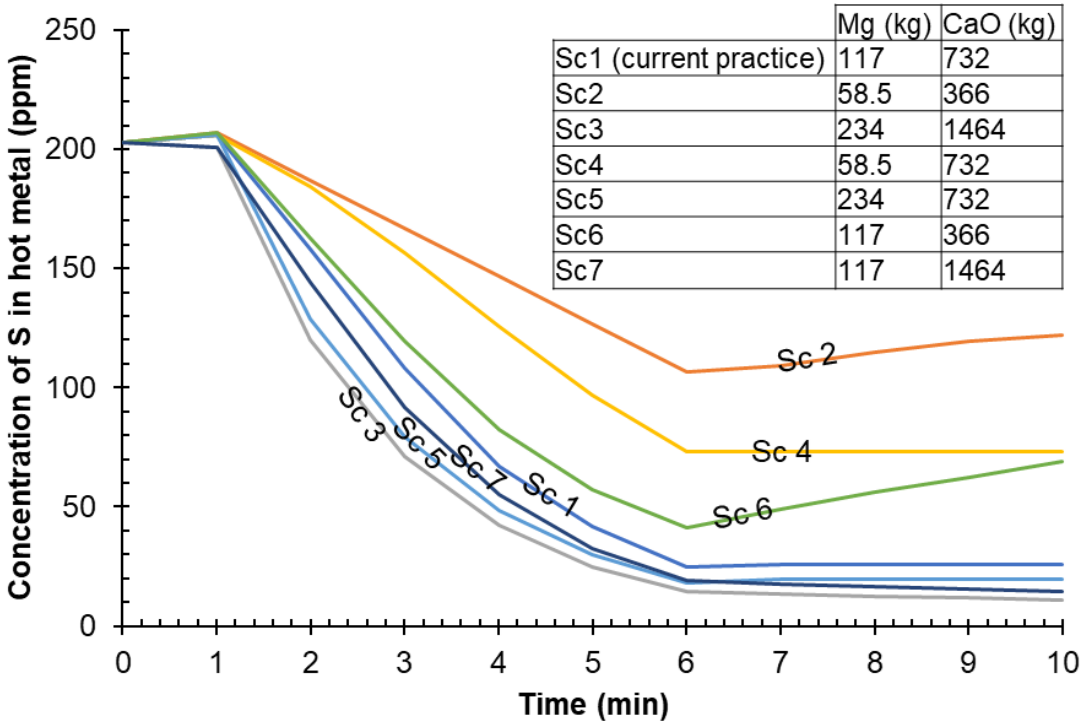

	Mg (kg)	CaO (kg)
Sc1 (current practice)	117	732
Sc2	58.5	366
Sc3	234	1464
Sc4	58.5	732
Sc5	234	732
Sc6	117	366
Sc7	117	1464

712
713 Fig. 10–Variation of sulfur contents in HM during powder injection process, simulated
714 with different flux addition scenarios. The general process conditions with the exception
715 of the added amount of flux are the same as that of heat #1 (see Table III).

716 As can be seen in scenarios 1 and 4, the soluble sulfur content in HM largely varies with
717 the amount of Mg flux. The difference in final sulfur content between scenario 1 (original
718 amount of Mg) and 4 (50% of original Mg) is very large. The final sulfur content in
719 scenarios 1 and 4 are 25 and 75 ppmw [S]. On the other hand, scenario 5 (200% Mg)
720 reaches to 20 ppmw [S]. This means that Mg is very important for desulfurization but there
721 is a certain maximum amount of Mg which is effective. Beyond this level, Mg addition is
722 unnecessary. This is easily understood from the chemical reaction of dissolution of Mg(g)
723 to Mg(l): Mg(g) = [Mg]. The maximum dissolution amount of Mg in plume zone of HM,
724 $[Mg]_{max}$, is dependent on the ferrostatic pressure at a given temperature.

Scenarios 1, 6 and 7 show the effect of the lime addition at a fixed Mg amount. As shown in Figure 10, decreasing lime content by half (scenario 6) increases the sulfur content to 69 ppmw, compared to 25 ppmw [S] produced from the original process condition (scenario 1). On the other hand, twice of lime addition (scenario 7) only slightly further decreases the sulfur content to 15 ppmw [S], but the difference is not very significant compared to the original operation condition. Scenarios 2 and 4, and scenarios 5 and 3 can also show the influence of lime amount at fixed Mg contents. In general, when Mg injected amount is smaller than the optimum quantity, the influence of lime on sulfur removal is significant, but when enough Mg is added to HM, the influence of lime on the final sulfur content is insignificant. These results support that Mg is a more effective desulfurization agent than lime, but lime itself can still contribute to a certain degree of desulfurization at plume zone, as also discussed above (see Figure 9 for contribution of three separate parameters, Mg, lime and top slag to desulfurization of HM).

In the injection process, the phase evolution of top slag is also important, as mentioned before. The final slag volume and final sulfur content of HM for different scenarios are plotted in Figure 11. As seen, scenarios 3 and 7 with the highest flux addition, respectively, have the lowest sulfur content of HM but simultaneously highest volume of top slag produced. The scenarios 5, 1, 4, 6 and 2 with the lowest amount of added flux, respectively, have higher sulfur content but simultaneously the lowest slag volume produced. Considering a specific target final sulfur of HM, scenarios 2, 4, and 6 are not acceptable. On the other hand, scenarios 3 and 7 have the highest slag volume, 100% and 86% more than heat #1 (scenario 1), respectively. Therefore, scenario 1 (the current operation) and scenario 5, which are very similar, seem to be the optimum cases.

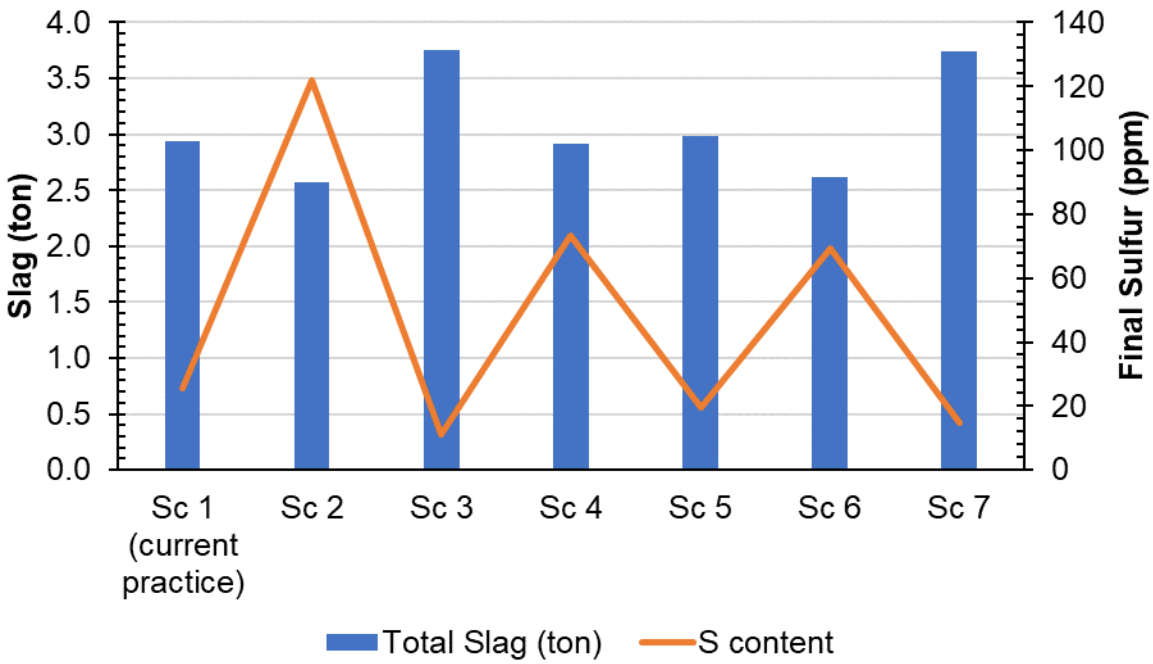

Fig. 11–Variation of slag volume (mass percent) in the final top slag (right axis) depending on the amount of flux added along with final sulfur content of hot metal (left axis).

Average liquid slag volume (mass percentage) of top slag during the process is plotted in Figure 12 for all the scenarios. It is seen that scenarios 2 and 6 with the lowest amount of added lime have the highest amounts of liquid slag volume however, the final S content of HM is not acceptable. Considering all the scenarios with desirable sulfur content of HM (1, 3, 5, 7), the scenarios 5 and 1 have the highest volume of liquid slag on the contrary to scenarios 3 and 7. Often colloid loss of iron is inversely related to the volume of liquid slag. That is, less iron is lost in the form of colloid to the top slag with high volume of liquid slag. On the other hand, it is projected that more iron is lost in the form of entrainment to the top slag with high volume of liquid slag. However, it has been reported that entrainment loss is often minimized via increasing the accuracy of the skimmer control, cleaning the skimmer paddle more often, or training the operator.[54] Therefore,

scenarios 1 and 5 are preferred to the scenarios 3 and 7 (*i.e.* less iron loss is estimated for the former ones).

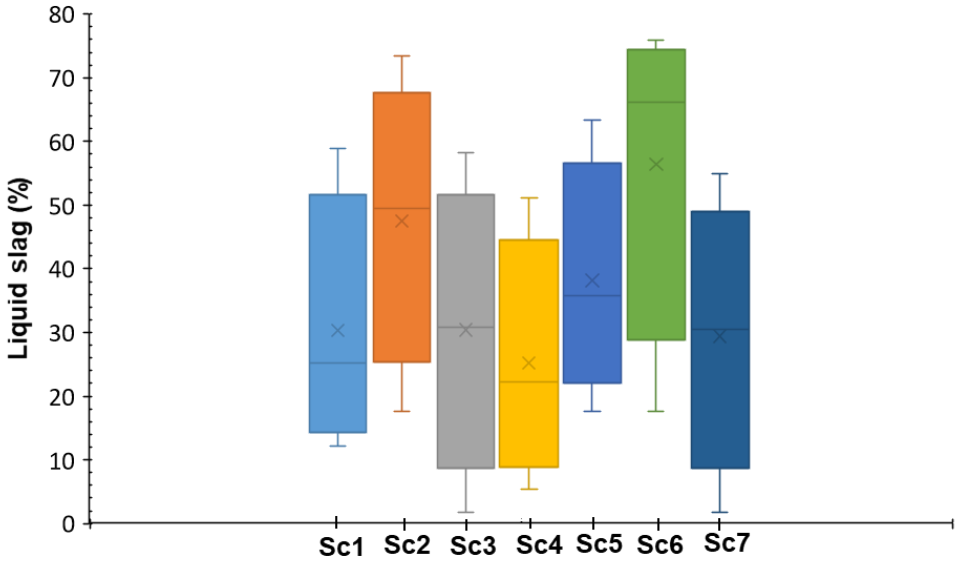

Fig. 12–Liquid slag volume (mass percentage) for various hot metal desulfurization scenarios (the description of each scenario has been given in figure 10).

In summary, considering the four criteria of target final sulfur content of HM, slag volume, amount of flux added, and iron loss; the scenario 1 (the current practice) can be concluded to be already quite an optimum condition. It should be noted that the current process conditions were obtained as the result of numerous trials and errors at the plant operation over several years. But using the present process simulation model, we can quickly find such optimum conditions. Therefore, the present process model can be used to search new optimum desulfurization process conditions based on certain economic constraints, and also be further developed to find the optimum process conditions using other types of flux for new smelting scenarios having different contents of S, C and Si, and slag chemistry in future without trials and errors.

6. Limitations of the present model

The present model assumed that there is no thermal gradient from the bulk HM to top slag, and both slag and HM are homogeneous in temperature. In reality, the temperature of slag and HM would not be homogeneous. In particular, the phase evolution of slag is very sensitive at around 1400 ^{o}C, the proper consideration of temperature would be necessary to describe the slag phase evolution in future. It is assumed that all reaction products including MgS and CaS and unreacted lime particles are absorbed by the top slag instantaneously. But in reality, there would be a delay of particle dissolution depending on temperature and slag composition, which would produce different type of sulfide and oxide reaction inclusion products. In the present model, we did not consider the occurrence of Ti(C,N) phase. Characterization of HM samples showed the accumulation of Ti(C,N) particles enriched in V in the HM top layer at the slag interface,[10] which also inhibit the assimilation of MgS to the top slag. In spite of such limitation, the desulfurization process was still reasonably taken into account in the present model, as demonstrated in the sections 4 and 5.

7. Summary

A kinetic model was developed for the hot metal pretreatment using submerged powder injection. All the general features of actual industrial operation were considered in the model. That is, the co-injection of magnesium and lime and the role of top slag during the

desulfurization process were modeled. The model was constructed based on the effective equilibrium reaction zone approach using the full power of FactSage thermochemical databases and macro processing code. Mathematical equations and empirical relations from the literature were critically evaluated and applied to the model to consider the process kinetics. The chemical evolution of hot metal and slag during the co-injection of lime and magnesium, predicted using the developed model based on initial conditions and process parameters, reasonably agreed with the plant data. The change in top slag chemistry during the process was estimated using the current model. The model was leveraged to investigate the possibility of further improving the desulfurization route at Tata Steel Europe. It was revealed the existing process is already close to an optimum condition. This model can be, therefore, used to optimize the process conditions and flux addition for hot metal with different qualities and sulfur, silicon and carbon contents, which is emerging in the coming decade.

Acknowledgements

Financial supports from Tata Steel Europe, Posco, Hyundai Steel, Nucor Steel, RioTinto Iron and Titanium, Nippon Steel Corp., JFE Steel, Voestalpine, RHI-Magnesita, SeAh Besteel, Doosan Heavy Industry and Construction and the Natural Sciences and Engineering Research Council of Canada are gratefully acknowledged. The authors would like to especially thank Tata Steel Europe for providing the plant data.

Conflict of Interest

On behalf of all authors, the corresponding author states that there is no conflict of interest.

References

1. Euro Inox: Stainless Steel: Tables of Technical Properties. Luxembourg, Euro Inox, 2007, pp. 25.

2. Euro-Asian Council for Standardization, M.a.C.E., GOST 5632-72, 2007, Minsk, Belarus.

3. R. W. Revie: Oil and Gas Pipelines, John Wiley & Sons, Hoboken, New Jersey, 2015, pp. 229.

4. J. W. K. Van Boggelen, H. K. A. Meijer, C. Zeilstra, and Z. Li: Scanmet V., Luleå, Sweden, 2016, pp. 1-10.

5. 30. G. A. Irons and R. I. L. Guthrie: *Can. Metall. Q.*, 1976, vol.15, pp. 325-32.

6. G. A. Irons and R. I. L. Guthrie: *Ironmaking Steelmaking*, 1981, vol. 8, pp. 114-21.

7. S. Ohguchi and D. G. C. Robertson: *Ironmaking Steelmaking*, 1984, vol. 11, pp. 262-73.

8. T. Kitamura, K. Shibata, I. Sawada, and S. Kitamura: *Proc. Sixth Int. Iron and Steel Cong.*, Nagoya, *ISIJ*, 1990, vol.3, pp. 50-6.

9. J. Yang, S. Ozaki, R. Kakimoto, K. Okumura, M. Kuwabara, and M. Sano: *ISIJ Int.*, 2001, vol. 41, pp. 945-54.

10. H.-J. Visser: Modeling of Injection Processes in Ladle Metallurgy, Ph.D. Thesis, 2016, TU Delft, the Netherlands.

11. M.C. Speer and N.A.D. Parlee: *Cast Met. Res. J.*, 1972, vol. 8, pp. 122-8.

12. E. T. Engh, H. , and Midtgaard, J. C. Borke, and T. Rosenquist: *Scand. J. Metall*., 1979, vol. 8, 195-8.

13. S. Ohguchi and D. G. C. Robertson: *Ironmaking Steelmaking*, 1984, vol. 11, 274-82.

14. S. Ban-Ya and M. Hino: *Tetsu-to-Hagane*, 1988, vol. 74, pp. 1701.

15. D. J. Sosinsky and I. D. Sommerville: *Met. Trans*., 1986, vol. 17B, pp. 331-7.

16. Tekkou-Binran: *Iron Steel Inst. Japan*, Tokyo, 1981, pp. 17-27.

17. M.-A. Van Ende, Y.-M. Kim, M.-K. Cho, J.-H. Choi, and I.-H. Jung: *Metall. Mater. Trans. B*, 2011, vol. 42, pp. 477-89.

18. I.-H. Jung, M.-A. Van Ende, W.-Y. Kim: *CAMP-ISIJ*, 2012, vol. 25, pp. 199-202.

19. M.-A. Van Ende and I.-H. Jung: *ISIJ Int*., 2014, vol. 54, pp. 489-95.

20. M.-A. Van Ende and I.-H. Jung: *Metall. Mater. Trans. B*, 2017, vol. 48, pp. 28-36.

21. E. Moosavi-Khoonsari, E. Zinngrebe, S. Van Der Laan, R. Kalter, and F. Mensonides: *4th Eur. Steel Technol. and Appl. Days* (*ESTAD*), 2019, Düsseldorf, Germany.

22. www.FactSage.com. Accessed September 2021.

23. H. Lachmund, Y. Xie, T. Buhles, and W. Pluschkell: *Steel Res*., 2003, vol. 74, pp. 77-85.

24. G. Ebneth and W. Pluschkell: *Steel Res*., 1985, vol. 56, pp. 513-8.

25. S. Mukawa, Y. Ueshima, M. Sano, J. Yang, and M. Kuwabara: *ISIJ Int*., 2006, vol. 46, pp. 1778-82.

26. D. Lindström, P Nortier and D. Sichen: *Steel Res. Int*., 2014, vol. 85, pp. 76-88.

27. J. Yang, K. Okumura, M. Kuwabara, and M. Sano, *ISIJ Int*., 2001, vol. 41, pp. 965-73.

28. E.T. Turkdogan: Fundamentals of Steelmaking, Book 656, The Institute of Materials, 1996, London, England, pp.124.

29. J. Yang, M. Kuwabara, T. Teshigawara, and M. Sano: *ISIJ Int*., 2005, vol. 45, pp. 1607-15.

30. A. Ender, H. Van Den Boom, H. Kwast, and H. Lindenberg: *Steel Res. Int.*, 2005, vol. 76, 562-72.

31. L. Yan, Z. Ting-an, M. Sano, W. Qiang, and H. J.-Cheng: *J. Iron Steel Res. Int*., 2011, S2, pp. 166-71.

32. G. A. Irons, C. W. Chang, R. I. L. Guthrie, and J. Szekely: *Metall. Mater. Trans. B*, 1978, vol. 9, pp. 151-4.

33. K. Yonezawa, S. Sasakawa, and S. Kitamura: *CAMP-ISIJ*, 1993, vol. 6, pp. 1070.

34. A. Aoyagi, Z. Mukuda, S. Takada, and S. Oomiya: *CAMP-ISIJ*, 1994, vol. 7, pp. 221.

35. T. Fujita, K. Matuo, and S. Nakasima: *CAMP-ISIJ*, 1994, vol. 7, pp. 218.

36. S. Yamaguchi, T. Uemura, H. Nashiwa, and H. Sugita: *Ironmaking Steelmaking*, 1977, vol. 4, pp. 276.

37. J. Yang, M. Kuwabara, K. Okumura, and M. Sano: *ISIJ Int*., 2005, vol. 45, pp. 1795-803.

38. W. F. Holbrook, C. C. Furnas, and T. L. Joseph: *Ind. Eng. Chem*., 1932, vol. 24, pp. 993.

39. R. E. Grace and G. Derge: *Trans. Met. Soc. AIME*., 1958, vol. 212, pp. 331-7.

40. A. Majdic, D. Graf, and H. Schenk: *Arch. Eisenhuttenwes*, 1969, vol. 40, pp. 627-30.

41. E. A. Brandes and G. B. Brook, Smithells Metals Reference Book, 7th ed., Reed Educational and Professional Publishing Ltd., 1992, Great Britain, pp. 1045-6.

42. N. W. Jones: *Ironmaking Steelmaking*, 1998, vol. 25, pp. 460-5.

43. K.C. Mills, L. Yuan, and R.T. Jones: *J. South. Afr. Inst. Min. Metall*., 2011, vol. 111, pp. 649 – 58.

44. T. Kai, K. Okohira, M. Higuchi, and M. Hirai: *Tetsu-to-Hagane*, 1983, vol. 69, pp. 228-37.

45. D. Oymo and R. I.L. Guthrie: *Proc. 4th Process Techno. Conf*., Warrendale, PA, 1984, pp. 45-52.

46. O. Haida, T. Emi, S. Yamada, and F Sudo: *Proc. SCANINJECT II Conf*., Luleä, Sweden, 1980, pp. 20:1-20:20.

47. S. Asai, T. Okarnoto, J. He, and I. Muchi: *Trans. ISIJ*, 1983, vol. 23, pp. 43-50.

48. O. Haida and J. K. Brimacombe: *Proc. SCANINJECT III Conf*., Luleä, Sweden, 1983, vol.1, pp. 5:1-5:15.

49. K. Nakanishi, T. Fujii. and J. Szekely: *Ironmaking Steelmaking*, 1975, vol. 2, pp. 193-7.

50. J. Szekely, T. Lehner, and C. W. Chang: *Ironmaking Steelmaking*, 1979, vol. 3, pp. 285-93.

51. U. P. Sinha and M.J. McNallan: *Metall. Mater. Trans. B*, 1985, vol. 16B, pp. 850-3.

52. D. Mazumdar and R. I. L. Guthrie: *Metall. Mater. Trans. B*, 1986, vol. 17B, pp. 725-33.

53. D. Mazumdar and R. I. L. Guthrie: *ISIJ Int*., 1995, vol. 35, pp. 1-20.

54. F. N.H. Schrama, E. M. Beunder, S. K. Panda, H. J. Visser, E. Moosavi-Khoonsari, A. Hunt, J. Sietsma, and R. Boom, Y. Yang: *Ironmaking Steelmaking*, 2021, vol. 48, pp.14-24.

Nomenclature

ΔG^o	standard Gibbs energy of reaction (kJ)
A	interface area between top slag and metal (m^2)
A_p	surface area of one flux particle (m^2)
C	Plume constant
d_p	particle diameter (m)
D	metal bath diameter (m)
D_m	diffusion coefficient in metal (m^2/s)
g	Acceleration due to gravity (m^2/s)
H	metal bath depth (m)
H_p	plume height (m)
k_m^t	overall mass transfer coefficient in metal for transitory reaction zone (m/s)
k_p^t	overall mass transfer coefficient in flux particle for transitory reaction zone (m/s)
k_m^p	overall mass transfer coefficient in metal for permanent contact reaction zone (m/s)
k_s^p	overall mass transfer coefficient in slag for permanent contact reaction zone (m/s)
L	lance immersion depth (m)
n_p	number of flux particles in plume
P^o	pressure on bath surface (atm)
P	overall pressure at the injection point
P_{MgS}	MgS solubility product
Q	gas flow rate (Nm^3/min)
R	gas constant (J/K-mol)
t_p	particle residence time (s)
Δt	calculation time step (s)
t_{mix}	time for 95% mixing
T	metal bath temperature (K)
T_m	metal melting temperature (K)
T_Q	gas temperature (K)
u	slip velocity between flux particle and melt (m/s)
U_m	metal mean rising velocity (m/s)
V_m^t	metal effective volume in transitory reaction zone (kg)
V_p^t	flux particle effective volume in transitory reaction zone (kg)
V_m^p	metal effective volume in permanent contact reaction zone (kg)
V_s^p	slag effective volume in permanent contact reaction zone (kg)
V_p	plume volume (m^3)
W_m	metal mass (ton)
W_P	particle injection rate (kg/s)
x	Plume vertical coordinate (m)

Greek symbols

β	fractional depth of lance submergence
δ	plume radius (m)
ε	mixing energy (W/kg)
μ_m	metal viscosity (pa-s)
ρ_m	metal density (kg/m^3)
ρ_m^o	metal density at melting point (kg/m^3)
ρ_p	flux particle density (kg/m^3)
ρ_s	top slag density (kg/m^3)
ρ_w	water density (kg/m^3)

934

935

Table I. Summary of the existing desulfurization models in comparison to the actual industrial practice.

	Top slag (chemistry and phase evolution)	**Flux**
Industrial DeS Practice	Yes	Mg + CaO
Irons & Guthrie[5,6]	No	Mg
Ohguchi & Robertson[7,13]	Yes (no phase evolution)	$CaO-Al_2O_3-CaF_2$
Kitamura[8]	Yes (no phase evolution)	$CaO-FeO_x-CaF_2$
Yang et al.[9]	No	Mg
Visser[10]	No	Mg + CaO
This Work	Yes	Mg + CaO

936

937

Table II. Model variables fitted to plant data.

Excess O_2(g) (added for Si oxidation) (kg/min)	0.01
Plume height - H_p (m)	0.2
Plume volume correction factor - C	3
Mixing time correction factor (α)	1
Calculation time step - Δt (s)	60

938

939

Table III. Process conditions and parameters used in the present simulation, taken from the reference.[10]

Plant data	**Heat 1**	**Heat 2**
Hot metal mass (ton)	288	283
Hot metal average temperature (^{o}C)	1370	1399
Initial / final S content (ppm)	203 / 7	229 / 7
Slag mass* (ton)	2	2
Slag density (g / cm^3)	2.8	2.8
Metal bath depth (m)	3.7	3.7
Vessel diameter (m)	4	4
Lance immersion depth (m)	3.2	3.2
Fractional depth of lance submergence	1	1
Mg efficiency (%)	51	43
Overall pressure at injection point (atm)	3.2	3.2
Lime particle density (g/cm^3)	3.3	3.3
Average lime particle diameter (μm)	110	110
Lime injection rate (kg/s)	1.74	1.73
Lime injection period (s)	420	420
Magnesium injection rate (kg/s)	0.39	0.48
Magnesium injection period (s)	300	300
Gas flow rate (Nm^3/s)	0.28	0.28
Gas feeding temperature (^{o}C)	25	25
Average mass transfer coefficient in metal - D_m (m^2/s)	10^{-9}	10^{-9}
Plume mass exchanged (%/Δt)	100	100

Hot metal composition (wt%)
Heat 1: S (0.0203) – Si (0.354) – Mn (0.419) – P (0.066) – Cr (0.025) – C (4.3)
Heat 2: S (0.0229) – Si (0.474) – Mn (0.421) – P (0.066) – Cr (0.025) – C (4.3)
Average slag composition (wt%)
CaO (38.8) – MgO (9.0) – Al_2O_3 (14.6) – SiO_2 (34.6) – CaS (2.4)

* Carryover slag mass cannot be measured (an estimated value).

940

941

Table IV. Calculated parameters using the present model.

	Heat 1	**Heat 2**
Plume volume – V_p (m^3)	17.1	17.1
Mixing energy - ε (W/kg)	0.7	0.7
Mixing time – t_{mix} (min)	0.9	0.9
Metal rising velocity – U_m (m/s)	5.4	5.4
Particle residence time – t_p (s)	0.6	0.6
Lime particle slip velocity - u (m/s)	83.0E-04	84.4E-04
Mass transfer coefficient in metal - k_m^t(m/s)	5.37E-04	5.41E-04
Mass transfer coefficient in metal - k_m^p (m/s)	3.43E-03	3.49E-03

942

943

944

945

Tables captions

Table I. Summary of the existing desulfurization models in comparison to the actual industrial practice.

Table II. Model variables fitted to plant data.

Table III. Process conditions and parameters used in the present simulation, taken from the reference.[10]

Table IV. Calculated parameters using the present model.

Figures captions

Fig. 1–Schematic diagram of hot metal pretreatment with powder injection.

Fig. 2–Effective equilibrium reaction zone (EERZ) concept for slag – metal reaction.

Fig. 3–Schematic diagram of the reaction zones in the present model of hot metal pretreatment (powder injection process).

Fig. 4–The overall calculation procedure of the presented model.

Fig. 5–Schematic presentation of the bubble plume.

Fig. 6–Solubility product of MgS, P_{MgS} = *[ppmw Mg] [ppmw S]*, in hot metal calculated using FactSage 7.3. Compositions of heat #1 and heat #2 are given in Table III.

Fig. 7–Simulated heat #1 (a), (b) hot metal composition, and (c) phase distribution in top slag. The symbols are plant data.[10] The lines were calculated from the present model. L, Mel, aC2S and C3MS2 stand for liquid slag, melilite, α-C_2S and $Ca_3MgSi_2O_6$, respectively.

Fig. 8–Simulated heat #2 (a), (b) hot metal composition, and (c) phase distribution in top slag. The symbols are plant data.[10] The lines were calculated from the present model. L, Mel, aC2S and C3MS2 stand for liquid slag, melilite, α-C_2S and $Ca_3MgSi_2O_6$, respectively.

Fig. 9–Separate contribution of magnesium, lime and top slag to the sulfur removal process, calculated from the present process model. Three simulations were performed based on heat #1.

Fig. 10–Variation of sulfur contents in HM during powder injection process, simulated with different flux addition scenarios. The general process conditions with the exception of the added amount of flux are the same as that of heat #1 (see Table III).

Fig. 11–Variation of slag volume (mass percent) in the final top slag (right axis) depending on the amount of flux added along with final sulfur content of hot metal (left axis).

Fig. 12–Liquid slag volume (mass percentage) for various hot metal desulfurization scenarios (the description of each scenario has been given in figure 10).